DOI 10.1007/s10946-019-09784-6
Journal of Russian Laser Research, Volume 40, Number 2, March, 2019

FAST 3D RECONSTRUCTION OF INDOOR SCENES USING HEIGHT-ADJUSTABLE MOBILE LIDAR

Shuaihao Li,[1†] Xinfeng Yang,[1] Bin Zhang,[2,3] Wenxing Li,[4] and Min Chen[1*]

[1]*School of Computer Science, Wuhan University*
Wuhan 430072, China
[2]*School of Remote Sensing and Information Engineering, Wuhan University*
Wuhan 430072, China
[3]*Department of Computer Science, City University of Hong Kong*
Hong Kong 999077, China
[4]*Chongqing Wanzhou Port Power Co., Ltd., Shenhua Shendong Power*
Chongqing 404000, China

*Corresponding author e-mail: chenmin @ whu.edu.cn
†Corresponding author e-mail: lishuaihao @ whu.edu.cn

Abstract

To enhance the model integrity in the fast three-dimensional (3D) reconstruction of complex indoor scenes, we propose an automatic acquisition method of point cloud data and RGB images at different heights, using height-adjustable mobile LIDAR (a system for light identification detection and ranging) for indoor scenes and design a complete reconstruction workflow. In the data acquisition and processing phases, some strategies and algorithms are used to eliminate the redundant data of a point cloud, which can effectively reduce the computation burden of subsequent processes such as the point cloud registration. Our experimental results further demonstrate that this method not only enhances the integrity of indoor scene models and visual effects of model roaming at different heights but also improves the speed and accuracy of 3D reconstruction.

Keywords: height-adjustable mobile LIDAR, point cloud, redundancy elimination, indoor scene, 3D reconstruction.

1. Introduction

In the 3D reconstruction of indoor scenes, the traditional methods of acquiring 3D coordinates by 2D image sequence often have many disadvantages, such as large amount of computation, long reconstruction time, complex process, and low efficiency. The LIDAR system can directly obtain the point cloud data of the target surface, which has many advantages such as high speed, high point cloud density, low cost, high precision of the model reconstructed, and so on.

However, the LIDAR is generally applied to large-scale areas such as outdoor scenes, buildings, or cities [1], where data acquisition is usually done by combining LIDAR with an unmanned aerial vehicle (UAV) or setting up multiple LIDAR around the target. For indoor scenes where the space is usually small, it is not feasible to set up multiple LIDARs, and the more LIDARs there are, the higher the cost of completing the 3D reconstruction. The combination of LIDAR and UAV for scanning is more difficult to realize indoors. On the other hand, if a single fixed LIDAR is used for data acquisition, the reconstructed

Manuscript submitted by the authors in English on November 11, 2018.

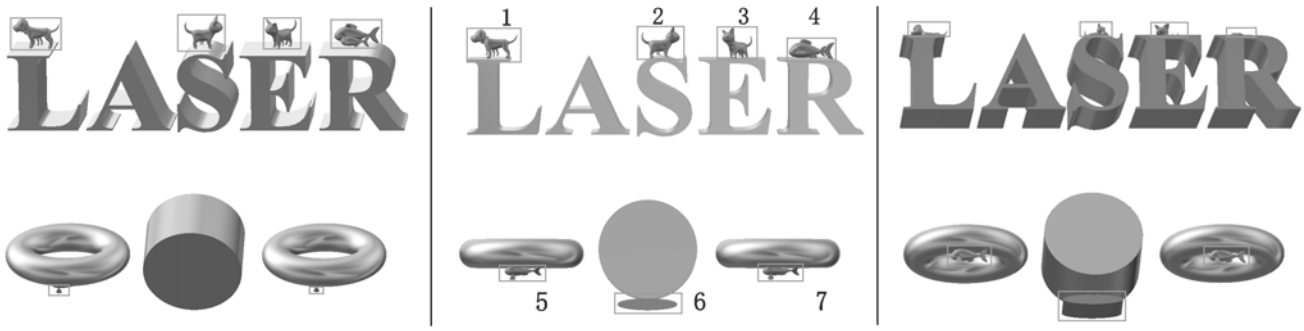

Fig. 1. Comparison of object integrity of scene scanned by LIDAR at different postures.

model often loses a lot of surface details due to its posture and position and other factors, thus lacking integrity [2].

In this paper, we acquire data by customizing a set of height-adjustable mobile robots and combining them with LIDAR to realize the integrity modeling of indoor scenes. By making the LIDAR move at the set path level, full scanning is carried out to ensure the integrity of the horizontal scene model. On the other hand, the vector of the LIDAR Y axis can automatically adjust itself to ensure the integrity of the scene model in the vertical direction. For redundant data scanned at different heights, we present an algorithm to eliminate the redundancy, which reduces the computation of the subsequent 3D reconstruction and improves the reconstruction efficiency.

The algorithm is verified in an indoor scene experiment. The results show that the algorithm is the fastest in terms of time efficiency and can be compared with the best algorithms in numerical and visual effects and even exceeds the best algorithms in some cases.

2. Design of 3D Reconstruction Workflow of Indoor Scene Based on Mobile LIDAR

After obtaining the point cloud and RGB (red, green, and blue) images of indoor scenes by LIDAR, the data are first preprocessed by denoising [3] and filtering [4, 5]. Then the point cloud thinning is used to eliminate excessive duplicate data [6] to minimize the number of data points, reduce subsequent computation, and save storage space. Since point clouds of many overlapping areas are generated during the data acquisition phase, it is necessary to identify and eliminate redundant data in these areas [7]. Since the original point cloud data and RGB images belong to the LIDAR coordinate system and the CCD coordinate system, respectively, it is necessary to convert them to the world coordinate system [8] for subsequent reconstruction. After completing the above work, these point cloud data are still local and scattered point cloud obtained from different positions, heights, and angles of view. There are rotation dislocation and translation dislocation among them; therefore, it needs to be combined by point cloud registration [9, 10]. For a multiple point cloud that has been registered, a complete point cloud model can be generated through the point cloud fusion [11], but the surface of the model is still a point cloud without topological structure, so it is necessary to construct a grid to generate the surface of the model. Finally, all the reconstruction processes are completed by texture mapping of RGB images [12].

This paper focuses on data acquisition of a full indoor scene and point cloud redundancy elimination of overlapped area.

3. Acquisition of Point Cloud and RGB Images

When using the traditional fixed LIDAR method to obtain the target data, the object on the surface of the scene cannot be scanned comprehensively due to the influence of the posture and position of the LIDAR and other factors, finally resulting in lack of integrity of the reconstructed 3D model. As shown in Fig. 1, the middle picture shows the display effect of the 3D model of the objects when the height of the LIDAR is the same as the object on the scene, and the left picture shows the display effect when the LIDAR is higher than the object on the scene, and the object is overlooked at an angle of 20°. The right one shows the display effect when the LIDAR is lower than the object on the scene, and the elevation angle is 20°. In conclusion, if the LIDAR is different from the height of the objects in the scene, there will be a situation where some objects cannot be scanned. For example, the data of some small objects below the cylinder and ring on the left-hand side of the picture (objects labeled 5–7) and above the stereoscopic character on the right-hand side of the picture (objects labeled 1–4) cannot be collected.

For this case, we optimize the LIDAR scanning method to enhance the integrity of the model.

3.1. Experimental Setup

In this paper, we adopt a customized height-adjustable mobile LIDAR system.

The main hardware includes:

A remote-controlled mobile robot covering an area of about 0.5 m^2 and a height of 190 cm, with a load-bearing platform capable of lifting and lowering to a height of 500 cm and an accurate inertial positioning system.

A dynamic differential GPS receiver used to determine the spatial position of the scanning projection center;

An inertial measurement unit (IMU) used for completely automatic positioning and velocity measurements and obtaining the posture data of the main optical axis of the LIDAR.

A linear scanning laser ranging system used to measure the distance from the LIDAR to the point on the scene, and then to calculate the 3D coordinate of the point on the scene according to the LIDAR coordinate. Its effective measuring range is 0.3–50 m, the scanning rate is 60,000 points per second, the angular resolution is $0.125'$ and the visual range is 360° horizontally and 270° vertically. It has a Wi-Fi hot spot function and a scanner that can operate remotely and wirelessly through an intelligent terminal [13].

A CCD camera system used to obtain the RGB images of the scene and finally to map the texture of the model. It consists of five cameras, one on the top, towards the vertical orientation, and four on the side, towards the horizontal orientation. The scanning area can be photographed in real time at 360° horizontally and 270° vertically, and a panoramic image of 2,200 pixels can be obtained.

3.2. Data Acquisition

The system first observes and analyzes the scene, formulates the measuring path, locates the initial point, then moves and collects the data according to the set path at the same time, according to the concave and convex situation of the scene surface; the system automatically adjusts the height of the bearing platform for full data collection. The inertial auxiliary positioning system locates the position of the real-time data acquisition equipment. The LIDAR and CCD camera system collect the point

cloud and RGB images of the indoor scene, respectively, and fuse the texture of the image with the corresponding point cloud in real time to obtain the color point cloud with 3D coordinate data.

The height adjustment method of the bearing platform is as follows. The system calculates the distance difference of the scene surface data acquired continuously while collecting, and when an abnormal value is found (exceeding the reference value 10 mm), it is judged that the scene surface has a convex part, and this part of the surface may produce shade caused by the low or high height of the laser light source, resulting in incomplete data collection. Then the system automatically stops moving and adjusts the height for multiple acquisition. The data acquisition workflow is shown in Fig. 2. Among them, for the reference value of the horizontal distance difference between two adjacent objects in the vertical direction, it can be set in advance. The smaller the value, the more comprehensive the scanning will be, the more complete the model, but the more redundant the data and computation. Therefore, setting of appropriate reference values is an important factor to ensure integrity and efficiency.

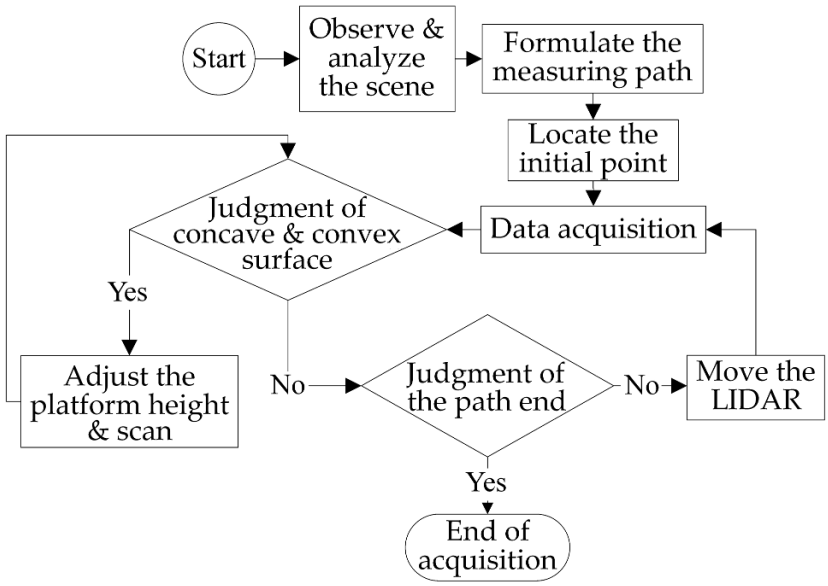

Fig. 2. Data acquisition workflow of indoor scene based on height-adjustable mobile LIDAR.

To reduce redundant data, only one data acquisition is performed on the upper scene at an initial height of 190 cm.

The data acquisition schematic of the indoor scene using the height-adjustable mobile LIDAR is shown in Fig. 3, with the overlooking view of an indoor scene (Fig. 3 A), where labels 1–7 indicate that there are convex objects on the wall at this position. When the system starts collecting data, the mobile robot moves according to the set path, while the LIDAR collects data of the scene surface. When the system moves to positions 1–7, the convex objects on the scene surface will be detected by the system, and the system adjusts the height and angle of the LIDAR and collects data. When the LIDAR height is lower than the convex object, the system raises the telescopic support and rotates the LIDAR downward to adjust its angle; the process is shown in Fig. 3 B. When the LIDAR height is higher than the convex object, the system reduces the telescopic support height and rotates the LIDAR upward to adjust its angle; the process is shown in Fig. 3 C. After all positions of the convex object are scanned, the robot continues to move along the set path until the system completes the acquisition of the entire scene surface.

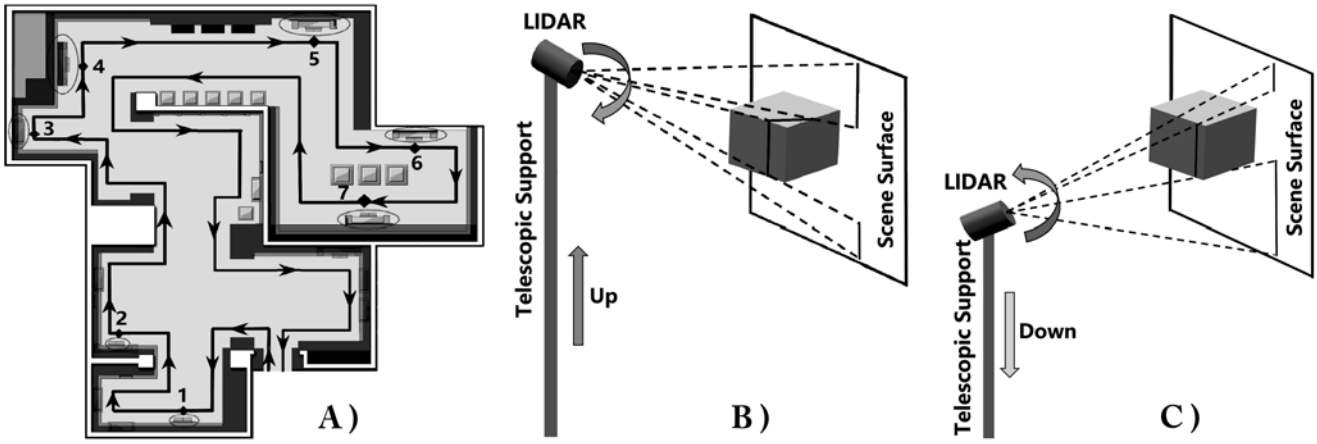

Fig. 3. Data acquisition schematic of indoor scene based on height-adjustable mobile LIDAR.

4. Redundancy Identification and Elimination of Point Cloud in Overlapped Area

For the high-density point cloud obtained, there is redundant data to some extent. There are two types of point cloud redundancy: complete overlap and partial overlap [14]. As shown in Fig. 4, if an irregular area is scanned by LIDAR twice or more, overlap of the point cloud will occur when the point clouds are registered. If the range of multiple scans is exactly the same, there is a complete overlap area shown on the left-hand side of Fig. 4. If the range of multiple scans is partially overlapped, there is a partially overlap area shown on the right-hand side of Fig. 4, where the rhombus and the circle represent the point cloud in different areas. The corresponding actual point cloud type is shown in Fig. 5, where the complete overlap area of the point cloud is in box B on the left-hand side, and the partial overlap area of the point cloud is in box C on the left-hand side.

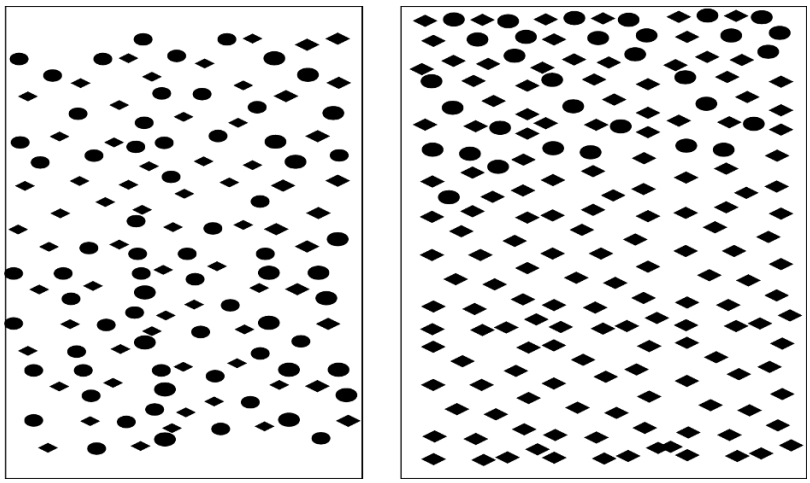

Fig. 4. Point cloud of two types of overlapping area: complete overlap (on the left) and partial overlap (on the right). The rhombus and the circle represent the point cloud in different areas, respectively.

We can identify whether there is overlap according to the RGB images corresponding to the point

cloud. If two adjacent RGB images have points of the same name [15], this means that the points are scanned at least twice, and the overlapping areas and redundant points can be determined. The judgment method of the same name point is to compare the distance between each echo in a single laser pulse, and if the distance is zero, the existence of the same name point is determined. For redundant points, the low-precision points in adjacent points are selected and eliminated [16, 17]. The process is as follows:

1). The maximum and minimum values of the three coordinates X, Y, and Z are retrieved in the point cloud of the scene corresponding to two adjacent RGB images; they are, respectively, denoted as $X_{\max}$, $Y_{\max}$, $Z_{\max}$, $X_{\min}$, $Y_{\min}$, $Z_{\min}$ and $X'_{\max}$, $Y'_{\max}$, $Z'_{\max}$, $X'_{\min}$, $Y'_{\min}$, $Z'_{\min}$. The cube bounding boxes of the area are set up using the difference between maximum and minimum of each coordinate axis as the side length, which is recorded as B_1 and B_2 respectively.

2). The points of area 2 are retrieved in the bounding box B_1 of area 1. If one point (X', Y', Z') in area 2 meets the conditions $X_{\max} > X' > X_{\min}$, $Y_{\max} > Y' > Y_{\min}$, and $Z_{\max} > X' > Z_{\min}$, this fact indicates that this point belongs to the overlapping area of B_1 and B_2.

3). The points of area 1 are retrieved in area 2 by the method of step 2.

4). Set up array $A_{[n]}$, the points in the overlapping part of areas 1 and 2 are stored in array $A_{[n]}$, where $A_{[n]}$ is the point cloud set P of overlapping area, and then the redundancy points are eliminated.

5). The weighted barycenter θ of all points in the point cloud set P are calculated using the down sampling algorithm. All the points in the area are replaced by the weighted barycenter θ, and θ are inserted into the point set P,

$$\theta^{'} = \sum_{j=1}^{k} \varpi(\theta) p_{ij} \left(\sum_{j=1}^{k} \varpi(\theta) \right)^{-1}, \tag{1}$$

where the weight is the Gauss function and $\varpi(\theta) = \exp\left(- \parallel p_{ij} - \theta \parallel^2 / r^2\right)$; the closer the distance from the barycenter, the greater the weight of the point and the smaller the weight of the point farther away; R is the size of the local neighborhood.

After traversing all areas, P^* is the point cloud data after down sampling, in which all redundant points in the overlapped area are eliminated.

5. Experimental Results

Figure 5 shows a comparison of the results of redundant points elimination in an overlapping area of an indoor scene using the above process and algorithm elaborated. The left-hand side of Fig. 5 shows the result of splicing the original point cloud in the overlapping area. The overlapping area of the point cloud is in box A, which is darker than other areas, and the density of points in it is about twice as high as other areas, because there are a lot of redundant points that have to be removed in it. The completely overlapping area of the point cloud is in box B, and the partial overlapping area is in box C. The right-hand side of Fig. 5 shows the result after eliminating the redundancy of the point cloud in the overlapping area (box A). On the left-hand side of Fig. 5, the original number of point clouds was 57,612, the number of redundant points was 12,671, and the removal rate was 22%. Therefore, the above algorithm cannot only eliminate the redundant points of overlapped areas but also preserve the original details of objects.

In addition, we compared the proposed method with other methods. As shown in Table 1, compared with the curvature sampling algorithm and the unified sampling algorithm [18], our algorithm maxi-

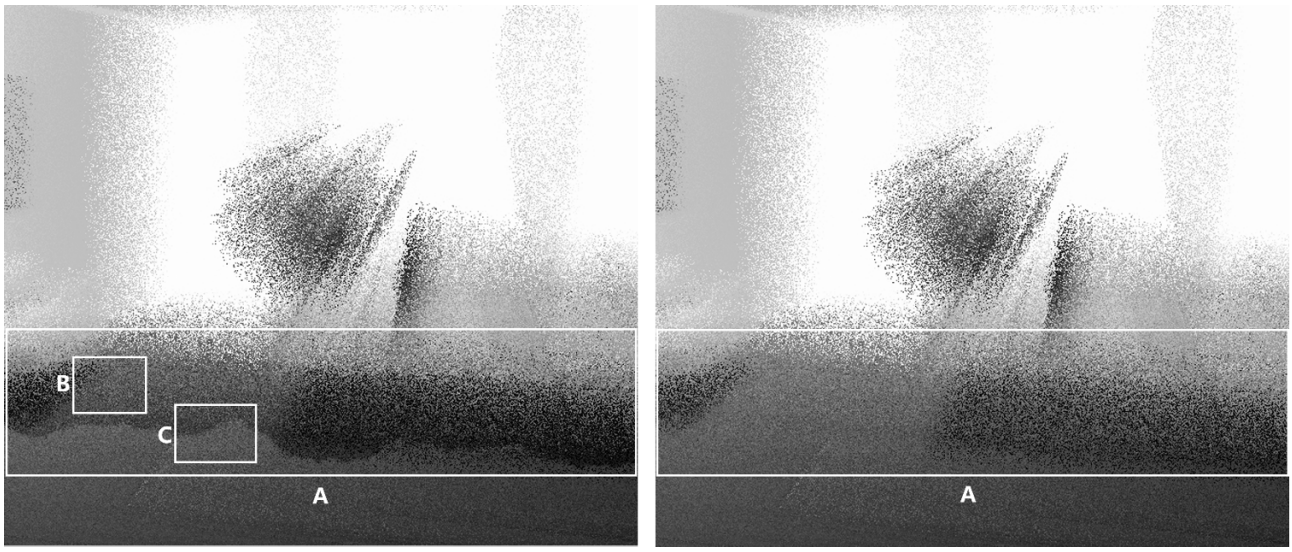

Fig. 5. The comparison before and after de-redundancy. Here, overlapping area (box A), complete overlap (box B), and partial overlap (box C).

mizes the removal efficiency of the redundant point cloud, and the computational complexity and time consumption of the algorithm are both small.

Table 1. Comparison of Experimental Results of Different Deredundancy Algorithms.

Method	Initial points	After removal	Points removed	Removal rate	Time, s
Uniform sampling	57,612	50,871	6,741	11.70%	3.982
Curvature sampling	57,612	48,855	8,757	15.20%	4.121
Our algorithm	57,612	44,941	12671	22%	3.577

The experimental results show that, compared with other algorithms, the removal efficiency of redundant data in the overlap area of the point cloud is optimized, and the advantage of lower time consumption is also obvious. Therefore, this greatly contributes to improving the accuracy of point cloud registration and fusion.

6. Conclusions

In this paper, we proposed a method of data acquisition using a height-adjustable mobile LIDAR. By automatically adjusting the height of the acquisition platform, the integrity of the 3D reconstruction of the indoor scene is ensured. The data of all scenes can be fully acquired by moving the LIDAR once according to the set path. By eliminating the redundant points in the overlapped area, the computation of the subsequent process is reduced, and the efficiency of reconstruction is improved. The results show that compared with the fixed laser scanning method, our data acquisition method can improve integrity in the 3D reconstruction of an indoor scene. Our method is better than other deredundancy algorithms in removal efficiency and time consumption of redundant data in the overlap area of the point cloud and

also enhances the visual effect of the model browsing at different heights.

However, this method remains to be improved. Due to the hardware limitation of the mobile robot with LIDAR, it has some shortcomings in 3D data acquisition and model reconstruction. For large indoor scenes, such as concert halls, auditoriums, shopping malls, and so on, which are higher than 6.5 m and where the mobile LIDAR platform cannot be set at this height, this method cannot be used for data collection. For large open indoor scenes, small UAVs can be selected for carrying LIDAR to obtain data. How to improve the system so that data of all indoor scenes can be collected is the focus of a follow-up study.

Acknowledgments

This study was funded by China National Mapping and Geographic Information Bureau Engineering Technology Research Center (ID:SIDT20170101) and Research Center for Culture–Technology Integration Innovation, Key Research Base of Humanities and Social Science of Hubei Province, China (ID:WK201704).

References

1. V. I. Grigorievsky, Y. A. Tezadov, and A. V. Elbakidze, *J. Russ. Laser Res.*, **38**, 344 (2017).
2. Y. Gong , W. Mao, J. Bi, et al., *Eng. Surveying Mapping*, **11**, 33 (2015).
3. S. Fleishman, I. Drori, and D. Cohenor, *ACM Trans. Graphics*, **22**, 950 (2003).
4. G. Sithole and G. Vosselman, *ISPRS J. Photogramm. Remote Sensing*, **59**, 85 (2004).
5. C. Tomasi and R. Manduchi, "Bilateral filtering for gray and color images," in: *Proceedings of the 6th IEEE International Conference on Computer Vision* (1998), p. 839.
6. K. Wang and L. Zheng, *Bull. Surveying Mapping*, **3** (2018).
7. H. Song and H. Y. Feng, *Comput.-Aid. Des.*, **40**, 281 (2008).
8. C. S. Fraser, *Photogramm. Eng. Remote Sensing*, **79**, 381 (2013).
9. D. G. Lowe, *Int. J. Comput. Vision*, **60**, 91 (2004).
10. M. Korn, M. Holzkothen, and J. Pauli, "Color supported generalized ICP," in: *IEEE International Conference on Computer Vision Theory and Applications* (2015), p. 592.
11. Y. Song, *Bull. Surveying Mapping*, **5**, 79 (2017).
12. E. Zhang, *ACM Trans. Graphics*, **24**, 1 (2005).
13. C. Tan, X. Fu, Y. Deng, et al., *J. Russ. Laser Res.*, **38**, 1 (2017).
14. J. G. Peng, H. C. Ma, J. W. Wu, et al., *Comput. Eng. Appl.*, **48**, 32 (2012).
15. Z. Zhang, R. Deriche, O. Faugeras, et al., *Artif. Intell.*, **78**, 87 (1995).
16. J. Chu, L. Feng, L. Wang, and G. M. Zhang, *Appl. Res. Comput.*, **30**, 6 (2013).
17. X. Y. Gu, *Research on the Key Technologies of Point Cloud Processing in 3D Reconstruction*, Yanshan University, Hebei (2015).
18. X. F. Lin, *Electron. Des. Eng.*, **11**, 23 (2012).